the capacitance determined by the depletion width (W_2) in a-Si:H instead of the thickness (L) of a-Si:H, as the measuring frequency decreases from 160 Hz, as long as the capacitance due to the trapping/detrapping processes is neglected. That is why the p-n junction analysis should be applied to discussing those C-V characteristics as will be described in the next section. In the figure, the capacitance measured at $V \leqq -2$ V is independent of the frequency, while the capacitance at $V \geqq -2$ V depends on the frequency, indicating that the information obtained in the range of $V \leqq -2$ V is unaffected by capacitances (e.g., diffusion capacitance) which results from the current flow across the heterojunction due to an ac voltage.

The low-frequency (<160-Hz) C-V characteristics are affected not only by the dielectric relaxation process but also by the trapping/detrapping process of electrons and holes between gap states and the extended states, indicating that the midgap-state density obtained from those low-frequency C-V characteristics depends on the measuring frequency. Furthermore, the simulation of their low-frequency C-V characteristics has been so difficult that the physical background of the apparent midgap-state density could not be understood clearly, as is similar to the case of Schottky barrier junctions. Although the zero-frequency C-V characteristics have been simulated because it is not necessary to consider the dielectric relaxation process and the trapping/detrapping process, those cannot experimentally be measured in fact. Since the high frequency enables us to neglect the dielectric relaxation process as well as the trapping/detrapping process, the simulation of the high-frequency C-V characteristics must be possible. Therefore, the C-V characteristics under a frequency much higher than 160 Hz have been measured and discussed in this chapter.

3-2-2. Steady-state heterojunction-monitored capacitance method

In order to understand the above results more clearly, a systematic study of undoped a-Si:H/p c-Si heterojunctions has been performed. Undoped a-Si:H films were deposited by the rf glow-discharge decomposition of pure SiH_4 on four kinds of p c-Si

(0.005-0.01, 0.1-0.15, 1-2, and 5-10 Ω cm) substrates heated to 250 ℃. Prior to a-Si:H deposition, silicon wafers were soaked in a solution of HF to remove SiO_2 and then rinsed in distilled water. A flow rate of 5 sccm and a gas pressure of 50 mTorr were maintained during the deposition. Mg was subsequently evaporated on the a-Si:H films in a vacuum of $7x10^{-7}$ Torr at room temperature. Table 3-1 summarizes Mg/undoped a-Si:H/p c-Si diodes used in the present work, where a film thickness (L) of a-Si:H, the resistivity (ρ_1) in p c-Si and the density (N_A) of acceptor impurities in p c-Si are listed. The value of N_A was determined by C-V measurements on Mg/p c-Si Schottky barrier diodes.

The C-V characteristics of these diodes have been measured at 100 kHz at room temperature. This frequency is high enough to be able to neglect the dielectric relaxation process in undoped a-Si:H (around 10^9 Ω cm in resistivity). Therefore, one can get information on the width of the depletion region extending in the p c-Si side regardless of that of the a-Si:H side. In fact, the capacitance of the diode (sample 5) using p^+ c-Si (0.005-0.01 Ω cm) measured at 100 kHz showed a constant value independent of the dc applied voltage, coinciding with that of the capacitance determined only by the film dimension of a-Si:H, i.e.,

$$C_2 = \varepsilon_{s2}/L \quad , \tag{3-1}$$

where ε_{s2} is the dielectric permittivity of a-Si:H and L is the thickness of a-Si:H measured by Talystep. It clearly indicates that the measuring frequency is higher than the reciprocal of the dielectric relaxation time of undoped a-Si:H, and besides, the depletion region is negligibly thin in the side of p^+ c-Si (0.005-0.01 Ω cm).

Figure 3.5 shows the $1/C^2$-V characteristics of sample 7 (1-2 Ω cm). The capacitance level of the diode replaced by p^+ c-Si of 0.005-0.01 Ω cm (sample 5) is also indicated in the figure by a broken line. Different from the conventional C-V theory, as is shown in the figure, $1/C^2$ is not proportional to the applied voltage.

TABLE 3-1. Various data of materials and diodes used in the present work. Experimental results obtained from C-V characteristics are also listed.

	p c-Si			undoped a-Si:H						
Sample number	ρ_1 (Ω cm)	N_A ($\times 10^{15}$ cm^{-3})	δ_1[a] (eV)	L (μm)	δ_2 (eV)	b	V_B (V)	N_I ($\times 10^{15}$ cm^{-3})	ΔE_C (eV)	χ_2[c] (eV)
2	5-10	2.0	0.22	1.16	0.72	C	0.31	6.2	0.13	3.92
3	1-2	9.0	0.18	0.80	0.76	C	0.51	3.6	0.33	3.72
4	1-2	9.0	0.18	2.19	0.72	C	0.37	2.8	0.15	3.90
5	0.005-0.01	——	0	1.02	0.72	C	——	——	——	——
6	0.1-0.15	180	0.10	1.02	0.72	C	——	——	——	——
7	1-2	9.0	0.18	1.02	0.72	C	0.42	3.9	0.20	3.85
8	5-10	2.0	0.22	1.02	0.72	C	0.38	4.0	0.20	3.85
9	1-2	9.0	0.18	1.77	0.84	I	0.37	1.6	0.27	3.78
10	5-10	2.0	0.22	1.77	0.84	I	0.20	1.8	0.14	3.91

[a] $\delta_1 = kT\ln(N_V/N_A)$, $N_V = 1.02\times10^{19}$ cm^{-3}.

[b] C:capacitively-coupled glow-discharge reaction chamber, I:inductively-coupled glow-discharge reaction chamber.

[c] χ_1 of 4.05 eV and E_{g1} of 1.12 eV are used to obtain χ_2.

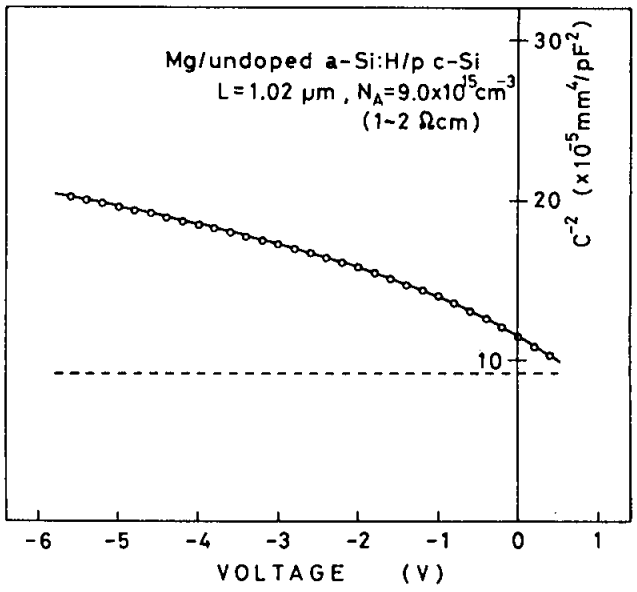

Fig.3.5. $1/C^2$-V characteristics of sample 7. The broken line is those of sample 5.

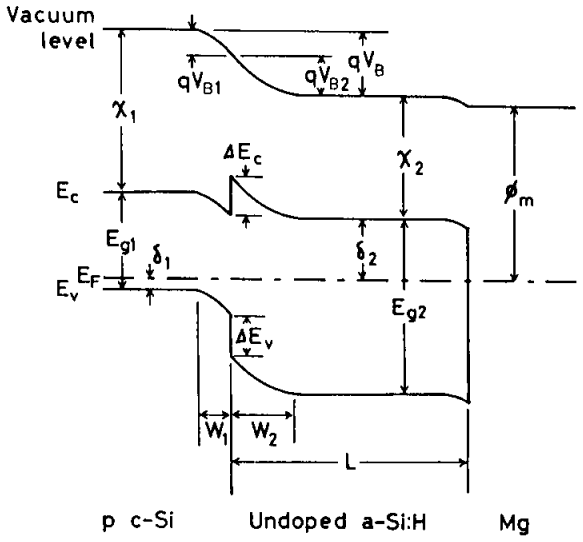

Fig.3.6. Energy-band diagram of p c-Si/undoped a-Si:H/Mg structure at equilibrium.

(A) p c-Si

(a) energy-band diagram

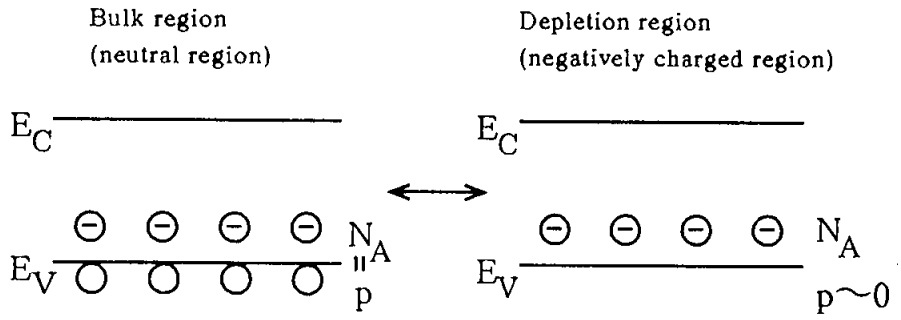

(B) undoped a-Si:H

(a) energy-band diagram

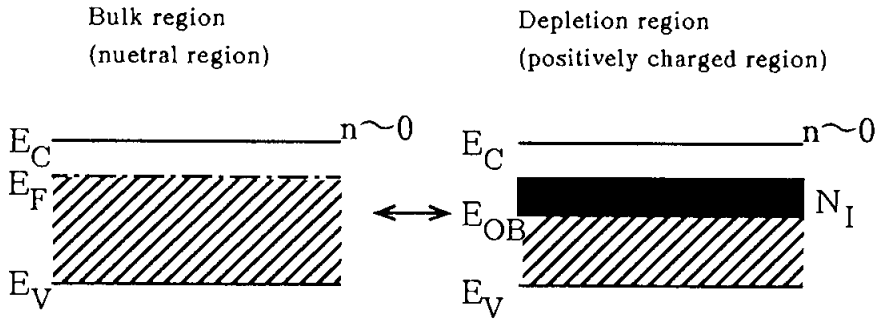

(b) density-of-state distribution [g(E)]

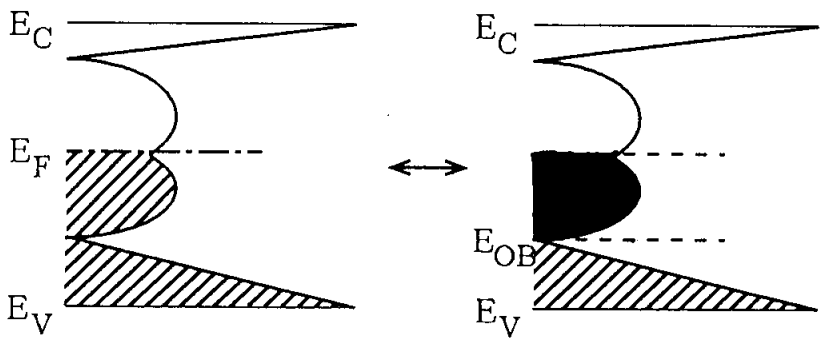

Fig.3.7. Changes of charged carriers and charged gap states between bulk and depletion regions in (a) energy-band diagrams and (b) density-of-state distributions for the cases of (A) p c-Si and (B) undoped a-Si:H. The symbols of ⊖ and ○ represent a negatively charged acceptor and a hole, respectively. The value of N_I is the amount of thermally emitted electrons per unit volume in the black area, which corresponds to the integration value of g(E) from E_{OB} to E_F. The gap states indicated by hatched areas are full of electrons.

The C-V characteristics in the figure is reasonably interpreted by assuming an ideal abrupt heterojunction without interface states. According to the abrupt heterojunction model, the present undoped (i.e., slightly n-type) a-Si/p c-Si heterojunction can be approximated by the energy-band diagram as is shown in Fig. 3.6, where χ is the electron affinity, V_B the built-in potential, δ the distance in energy from the Fermi level to the nearest band edge, E_g the energy-band gap of the semiconductor, W the width of the depletion region, L the thickness of a-Si:H, ΔE the different in energy between band edges of the two semiconductors, and ϕ_m the work function of Mg. The subscripts 1 and 2 refer to p c-Si and undoped a-Si:H, respectively, and the subscripts C and V refer to the conduction band and the valence band, respectively.

The depletion regions formed by the undoped a-Si:H/p c-Si heterojunction are considered. When a reverse bias voltage (V) is applied, it makes the space-charge regions both in a-Si:H and c-Si wider. Under the assumption that this p c-Si has only shallow acceptors, the space charge in p c-Si is formed by negatively charged acceptors and the space-charge density in p c-Si becomes N_A, as shown in Fig. 3.7(A). However, the amorphous component possesses gap states. Origin of the space charge in a-Si:H is schematically discussed using Fig. 3.7(B). In the bulk region, all the gap states below the Fermi level (E_F) are approximately considered to be occupied by electrons, while in the depletion region the states above E_{OB} indicated by the black area are approximately considered to be vacant of electrons, where E_{OB} is determined by thermal-emission rates for electrons and holes from gap states to the extended states and is given by (See Appendix)

$$E_{OB} = E_V + E_{g2}/2 + (kT/2)\ln(\nu_p/\nu_n) \quad . \qquad (3\text{-}2)$$

Here, ν_p and ν_n are the attempt-to-escape frequencies for holes and electrons, respectively. Since the difference between the bulk region and the depletion region is based on the change of electron occupation in the black area in the figure, the gap

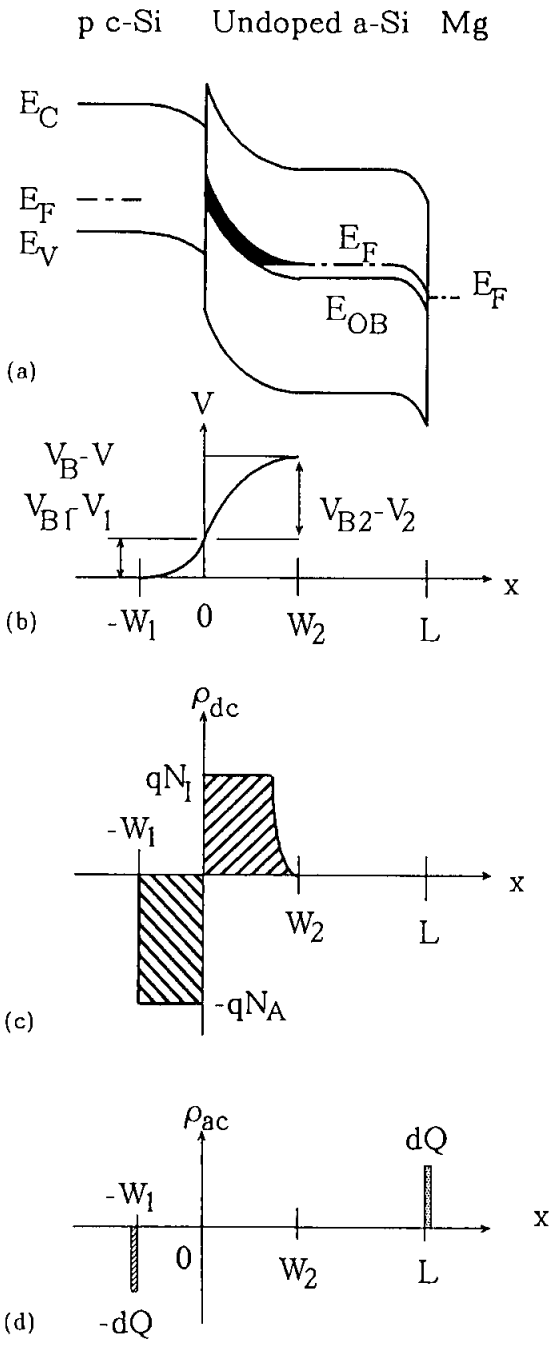

Fig.3.8. Schematic sketches of heterojunction: (a) energy-band diagram; (b) potential variation; (c) space-charge density for a reverse dc voltage; (d) charge in response to a small 100-kHz ac voltage to measure capacitance. The gap states indicated by the black area of (a) behave as positively charged states.

states in the black area behave like positively charged states, referred to as donorlike states, and N_I represents the density of the donorlike states. Therefore, the space-charge density is equal to the midgap-state density [i.e., the integration value of g(E) from E_{OB} to E_F]. So, N_I is referred to as a space-charge density as well as a midgap-state density in these undoped films.

Figure 3.8 shows schematic sketches of the heterojunction. The gap states in the black area in Fig. 3.8(a) behave like positively charged states. Figure 3.8(b) shows the potential variation with distance where V_B is the built-in potential. The depletion width (W_1) in p c-Si is given by[8)]

$$W_1 = [2\varepsilon_{s1}(V_{B1} - V_1)/qN_A]^{1/2} \tag{3-3}$$

and the depletion width (W_2) in a-Si:H is expressed as

$$W_2 \fallingdotseq [2\varepsilon_{s2}(V_{B2} - V_2)/qN_I]^{1/2} \tag{3-4}$$

and the charge neutrality in the heterojunction is described by

$$qN_AW_1 \fallingdotseq qN_IW_2 \quad . \tag{3-5}$$

The capacitance is measured using a small ac voltage of 100 kHz. The resistivity (ρ_1) of p c-Si used in this study is lower than 10 Ω cm so that the dielectric relaxation time ($\varepsilon_{s1}\rho_1$) becomes 10^{-11} s, indicating that the redistribution of holes (majority carriers in p c-Si) can respond to the 100-kHz ac voltage. The capacitance (C_1) in c-Si, therefore, is given by

$$C_1 = \varepsilon_{s1}/W_1 \quad . \tag{3-6}$$

On the other hand, the value of resistivity (ρ_2) for undoped a-Si:H is about 10^9 Ω cm. Then, the dielectric relaxation time becomes 10^{-3} s, suggesting that the redistribution of electrons (majority carriers in undoped a-Si:H) cannot respond to the ac voltage higher than 160 Hz. Thus, the undoped a-Si:H is considered as a dielectric material in its behavior in the case

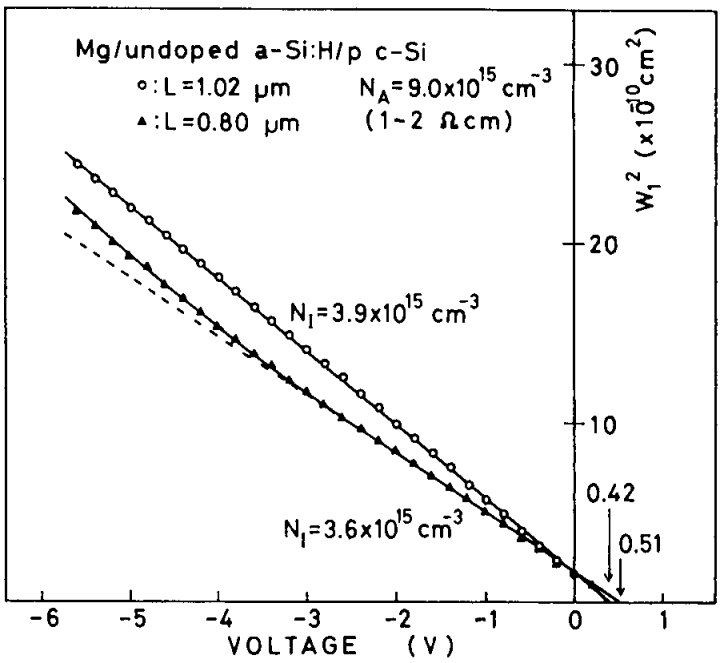

Fig.3.9. Width (W_1) of depletion region in c-Si as a function of voltage for sample 3 (L=0.80 μm) and 7 (L=1.02 μm).

of the 100-kHz ac voltage, indicating that the capacitance (C_2) in a-Si:H should be expressed by

$$C_2 = \varepsilon_{s2}/L \quad . \tag{3-7}$$

The measured capacitance (C) at 100 kHz is from a series of C_1 and C_2, and is given as

$$1/C = 1/C_1 + 1/C_2 \quad , \tag{3-8}$$

because spatially the redistribution of charged carriers can respond to the 100-kHz ac voltage at W_1 and L, as shown in Fig. 3.8(d). From Eqs. (3-3)-(3-5), the following relation is derived;

$$(V_{B1} - V_1)/(V_{B2} - V_2) \fallingdotseq N_I \varepsilon_{s2}/N_A \varepsilon_{s1} \quad . \tag{3-9}$$

The final equation is obtained as

$$W_1^2 = \varepsilon_{s1}^2(1/C - 1/C_2)^2 \tag{3-10}$$

$$\fallingdotseq 2\varepsilon_{s1}\varepsilon_{s2}N_I(V_B - V)/qN_A(N_A\varepsilon_{s1} + N_I\varepsilon_{s2}) \quad , \tag{3-11}$$

from Eqs. (3-3), (3-6), (3-8) and (3-9). As is clear from Eq. (3-11), the values of N_I and V_B can be graphically determined from the slope and the intercept on the abscissa, respectively, which is called a steady-state heterojunction-monitored capacitance (HMC) method.

Figure 3.9 shows the W_1^2-V characteristics of sample 7 (open circle), which was replotted from the data of Fig. 3.5. The data reveals quite a good linear relationship, indicating that the abrupt heterojunction model is applicable to the present system consisting of amorphous/crystalline heterolayer structure. The magnitudes of N_I and V_B are graphically determined from Eq. (3-11), which are listed in Table 3-1.

The thickness dependence of the W_1^2-V characteristics is investigated. The similar plot for sample 3 (solid triangle) is

also shown in Fig. 3.9, which is deviated from the straight line. This apparent invalidity of Eq. (3-11) simply originates from a thinner undoped a-Si:H layer (0.8 μm thick). The depletion layer spreads over the whole a-Si:H (i.e., W_2=L) when the reverse bias voltage exceeds some critical value, resulting in an upward break of the characteristic curve because much more fraction of reverse bias voltage is supported in p c-Si than that expected from Eq. (3-9). On other words, the slope of the W_1^2-V characteristics changes from $2\varepsilon_{s1}\varepsilon_{s2}N_I/qN_A(N_A\varepsilon_{s1}+N_I\varepsilon_{s2})$ to $2\varepsilon_{s1}/qN_A$ as the reverse bias voltage increases from the critical value to higher reverse bias. Using the value of N_I obtained from sample 7, the critical bias voltage, at which W_2 reaches to L (0.8 μm) for sample 3, was calculated as around -2 V, being in good agreement with the data in the figure.

The dependence of N_I on the p c-Si resistivity is studied. The undoped a-Si:H films of samples 5-8 were deposited simultaneously on four different p c-Si substrates. The capacitances of samples 5 and 6 (lower resistivities of p c-Si) were independent of the applied voltage, resulting from the formation of the wide depletion region only in the side of a-Si:H because N_A is much larger than N_I. On the other hand, the value of N_I obtained from sample 7 with the p c-Si resistivity of 1-2 Ω cm coincided with that of sample 8 with the resistivity of 5-10 Ω cm. And also the undoped a-Si:H films of samples 9 and 10 were deposited simultaneously by the inductively-coupled rf glow discharge on two different p c-Si substrates. Both of N_I were quite similar, as shown in Table 3-1.

From the studies of the thickness- and resistivity-dependencies, the steady-state HMC method is considered to be reasonable for the present heterojunctions. From the resistivity-dependence, one had better select p c-Si with N_A which is close to the value of N_I, indicating that several p c-Si substrates should be used in order to estimate N_I in the case that N_I is unknown at all.

3-2-3. Band discontinuity between a-Si:H and c-Si

Knowing band discontinuities at amorphous/crystalline